Probing two-center interference in H_2^+ using chirped pulses

Sigurd Askeland* and Morten Førre†
Department of Physics and Technology, University of Bergen, N-5007 Bergen, Norway

The influence of intermediate resonant dissociative channels in the few-photon ionization dynamics of H_2^+ is demonstrated in a pump-probe scenario. Two-photon ionization of H_2^+ by two sequentially applied pump and probe vuv/fs 10^{11} W/cm^2 laser pulses is reported. The kinetic energy distribution of the ejected protons is calculated by solving the time-dependent Schrödinger equation within the Born-Oppenheimer approximation, including the electronic three-dimensional and vibrational one-dimensional motion. Population is effectively transferred from the $1s\sigma_g$ to the $3p\sigma_u$ potential surface, via resonant one-photon absorption, by applying a chirped pump pulse. The molecule is ultimately ionized by the probe pulse. It is found that a double-peaked structure appears in the resulting kinetic energy release spectra of the nuclear fragments. A corresponding modulated structure also appears in the dissociative channels, merely demonstrating that the double-peaked structure in the spectra originates from the molecular $1s\sigma_g$-$3p\sigma_u$ electronic dynamics, and an inherent two-center interference in the underlying electric dipole coupling. It turns out that the dipole coupling between the $1s\sigma_g$ and $3p\sigma_u$ electronic states vanishes at an internuclear distance of 2.25 a.u., i.e., close to the equilibrium internuclear separation. The resulting node in the R-dependent dipole coupling imposes a minimum in the corresponding kinetic energy release spectra of the dissociating nuclei. By creating a negative or positive chirp in the applied pump pulse, it is found that the modulations can be made more or less salient.

PACS numbers: 33.80.Rv, 33.80.Gj, 82.53.Eb

INTRODUCTION

The hydrogen molecular ion (H_2^+), with its two protons bound together by a single electron, represents the simplest system in nature exhibiting the chemical bond. Due to its genuine and simple three-body structure, the interplay between electronic and nuclear degrees of freedom, in response to ionizing laser pulses, can be studied at the most fundamental level. As such, it has received considerable attention over the years, both theoretically and experimentally. Great effort has been put into unveiling various mechanisms responsible for the breakup of such light molecules subjected to laser pulses of femtosecond (fs) duration, and of varying intensity and central frequency, from the near infrared to the vuv and xuv regime. In this respect, the fs regime is particularly interesting as the nuclear (vibrational) motion of molecules typically occurs on this time scale. Since the pioneering work of Zewail [1], visualization of the full dynamical evolution of molecular wave packets has received a lot of attention.

The interplay of electronic levels, i.e., the $1s\sigma_g$ and $2p\sigma_u$ electronic states, in the strong-field multiphoton ionization dynamics of H_2^+, was recently investigated both experimentally [2, 3] and theoretically [4, 5], applying near-infrared laser pulses a few tens of fs of duration. The observed modulations in the resulting kinetic energy release (KER) spectra of the Coulomb exploding nuclei were interpreted as a multiple pathway interference effect [3]. A similar electronic quantum interference process was proposed as a mechanism for electron localization in dissociating H_2^+ [6]. Structures in the KER spectra, taking the form of a sequence of peaks, were also observed in other related experiments [7, 8]. The importance of multiple paths leading to the same final state becomes particularly pronounced in the ionization and dissociation dynamics of molecules, as the nuclear dissociative motion typically occurs on a completely different time scale than the electronic one. Hence, provided the pulse duration is comparable with the vibrational period of the given molecule, and that the laser pulse launches wave packets on several intermediate potential surfaces, e.g., the $1s\sigma_g$ and $2p\sigma_u$, the possibility of observing multiple pathway interference patterns is always present. Applying vuv/fs pulses, similar interference fringes were observed in the process of three-photon ionization of H_2^+, via resonant one- and two-photon absorption to the $2p\sigma_u$ and $3d\sigma_g$ potential curves [9]. Furthermore, in a recent work, various types of nuclear interference on the population of the dissociative channels $2s\sigma_g$ and $3d\sigma_g$ were discussed in detail [10]. It is also known that the ionization of H_2^+ by xuv laser pulses shows a strong dependence on the internuclear separation [11, 12], an R-dependence that can be interpreted in terms of two-center interference effects [11].

A perhaps less studied effect that may cause modulations in KER spectra, is the vanishing electric dipole coupling between pairs of electronic potential curves at particular internuclear separations. The signatures of such nodes in the dipole coupling may appear as characteristic minima in the resulting KER spectra. In the present work, we study theoretically the effect of a node in the electric dipole coupling between the $1s\sigma_g$ and $3p\sigma_u$ potential surfaces in H_2^+, in a pump-probe scenario. The zero in the coupling is positioned at $R = 2.25$ a.u., i.e., in the immediate neighborhood of the molecular equilibrium. As such, it is expected to play an essential role for the underlying ionization dynamics in the case of resonant $1s\sigma_g$-$3p\sigma_u$ absorption. In the present setup, a nuclear wave packet is launched onto the $3p\sigma_u$ potential surface by applying a resonant pump pulse. Then, at some given delay a second pulse, the probe, ionizes the excited wave packet, and the KER spectrum of the correlated nuclear fragments is extracted. The spectra are retrieved by solving

the time-dependent Schrödinger equation within the Born-Oppenheimer separation, including three electronic and one nuclear (vibrational) degrees of freedom. Two different initial vibrational wave packet are used in this work. Either the initial state is modeled to be the wave packet resulting from a vertical (Franck-Condon) transition from the H_2 $X^1\Sigma_g^+(v=0)$ ground state towards a superposition of vibrational states on the $1s\sigma_g$ potential surface of H_2^+. Alternatively, the $1s\sigma_g(v=0)$ vibrational ground state of H_2^+ is used. It is found that a clear signature of the node is imprinted into the final kinetic energy distribution of the Coulomb exploding nuclei. We attribute the resulting minimum in the KER to a kind of two-center interference stemming from the presence of nodes in the electronic wave functions. They give rise to corresponding nodes in the electronic dipole coupling. By varying the chirp of the pump pulse it is also demonstrated that the interference pattern can be made more or less distinct.

THEORY

The time-dependent Schrödinger equation (TDSE) is solved for the H_2^+ molecule exposed to a laser pulse. Using the Born-Oppenheimer approximation [13], we represent the electron part in full dimensionality, while allowing the nuclei to move along the internuclear axis. When propagating the H_2^+ molecular system in time, the electronic wave function is expanded in the field free electronic eigenfunctions. These eigenfunctions are obtained by solving the time independent Schrödinger equation (TISE) in the electronic coordinates, given as

$$\widehat{H}_{el}\psi_i^{el}(\mathbf{r};R) = E_i(R)\psi_i^{el}(\mathbf{r};R), \tag{1}$$

where the electronic Hamiltonian is

$$\widehat{H}_{el} = -\frac{1}{2}\nabla^2 - \frac{1}{r_1} - \frac{1}{r_2} + \frac{1}{R}, \tag{2}$$

expressed in atomic units. Here, $R = |\boldsymbol{R}|$ is the internuclear distance, $\boldsymbol{R}$ the internuclear vector, and $r_1 = |\boldsymbol{r} + \boldsymbol{R}/2|$ and $r_2 = |\boldsymbol{r} - \boldsymbol{R}/2|$ are the distances between the electron and the first and second nuclei, respectively. When working with two-center problems it is convenient to introduce prolate spheroidal coordinates (ξ, η, ϕ), defined by

$$\xi = (r_1 + r_2)/R, \qquad \eta = (r_1 - r_2)/R \tag{3}$$

The ϕ coordinate is the azimuthal angle, as in spherical coordinates. The electronic wave function is expanded in a product basis,

$$\psi^{el}(\xi,\eta,\phi) = \sum_{m,\mu,\nu} a_{m,\mu,\nu} U_\nu^m(\xi) V_\mu^m(\eta) \frac{e^{im\phi}}{\sqrt{2\pi}}, \tag{4}$$

as done by Kamta and Bandrauk in [14]. The radial basis function is given by

$$U_\nu^m(\xi) = N_\nu^m e^{-\alpha(\xi-1)}(\xi^2-1)^{|m|/2} L_{\nu-|m|}^{2|m|}[2\alpha(\xi-1)], \tag{5}$$

where $L_p^q(x)$ is a Laguerre polynomial, and $\alpha = \beta R$ is a parameter for complex scaling. In this work $\beta = 1$, however, making this a real function. The angular basis functions are defined as

$$V_\mu^m(\eta) = M_\mu^m P_\mu^m(\eta), \tag{6}$$

where $P_p^q(x)$ is the associated Legendre function. The normalization factors are

$$N_\nu^m = \sqrt{(2\alpha)^{2|m|+1}\frac{(\nu-|m|)!}{(\nu+|m|)!}} \tag{7}$$

and

$$M_\mu^m = \sqrt{\left(\mu+\frac{1}{2}\right)\frac{(\mu-m)!}{(\mu+m)!}} \tag{8}$$

The radial basis functions are not orthogonal, and both the Hamiltonian and the overlap matrix must therefore be calculated. The angular part of the matrix elements is given by analytical expressions, but the integrals over ξ must be done numerically (see appendices in [14]). As these integrals fit the bill for Gauss-Laguerre quadrature integration, this can be done efficiently and well. This quadrature formula requires the nodes of the Laguerre polynomials, which can be a challenge to obtain for high degree polynomials. Diagonalization of the Jacobi matrix, for instance, gave us good values only up to approximately degree 16, and the Python implementation of Laguerre polynomial evaluation became inaccurate in the same range. The most reliable approach was to get an estimate of the nodes, and then apply Newton's method, using the recurrence relation to evaluate the polynomials. For the electronic basis approximately 70 radial basis functions ($\nu_{max} = 71$), and 30 angular basis functions ($\mu_{max} = 31$) are used. Since the electric fields in this work are always parallel to the internuclear axis, the azimuthal symmetry is never broken, and including the $m = 0$ basis functions are sufficient. Our approach differs from [14] in that we solve the TISE for a range of different internuclear distances, R, in order to include vibrational nuclear motion in our model. This means that the basis functions, which become R-dependent, had to be set up individually for each value of R.

The electronic eigenfunctions are sorted according to the number of nodes in the η dimension, denoted by the number q. In the limit $R \to 0$, this number equals the orbital momentum quantum number l. Tests showed that at $q_{max} = 3$ the results were adequately converged in our simulations.

The dipole coupling matrix elements for a z-polarized laser field are given as

$$\left\langle \psi_i^{el} \middle| \frac{R\xi\eta}{2} \middle| \psi_j^{el} \right\rangle. \tag{9}$$

Their calculation is described in [14].

For the nuclear motion, a B-spline basis with 400 equidistantly distributed splines, stretching from $R = 0.5$ a.u. to

$R = 18.5$ a.u, are used [15, 16]. This was more than sufficient for the pulse durations used in this work.

The H_2^+ system is initially prepared either in its vibrational ground state, $1s\sigma_g(v=0)$, or in a Franck-Condon wave packet obtained by projecting the vibrational ground state wave function of H_2 onto the vibrational states in the H_2^+ $1s\sigma_g$ channel. The latter is meant to emulate H_2^+ as it is produced from H_2 in experiments, assuming that a direct vertical Franck-Condon transition from the H_2 vibrational ground state has taken place at time $t = 0$. The system is then propagated in time with an adaptive multistep predictor-corrector method [17].

In the calculations, the dipole approximation is undertaken, and the laser fields are assumed to be of Gaussian shape,

$$E(t) = E_0\sqrt{\frac{\tau_0}{\tau}}\exp\left[-\frac{2\ln 2(t-t_i)^2}{\tau^2}\right] \tag{10}$$

$$\times\cos\left[\omega(t-t_i)+\frac{2\ln 2(t-t_i)^2\eta}{\tau^2}\right] \tag{11}$$

The chirp parameter η enables us to delay either low frequency components, ($\eta < 0$), or high frequency components, ($\eta > 0$). E_0 is the amplitude of the electric field, ω is the central frequency of the pulse, t_i is the time when the pulse peaks, and τ_0 and $\tau = \tau_0\sqrt{1+\eta^2}$ are the FWHM pulse durations of the non-chirped and chirped pulses, respectively.

The KER spectrum, corresponding to dissociation of the molecule, is extracted from the propagated wave function by projecting onto the Born-Oppenheimer eigenstates, $\Psi(r,R) = \psi^{el}(\mathbf{r};R)\chi(R)$. The vibrational eigenfunctions, $\chi(R)$, are found by diagonalizing the nuclear TISE,

$$\left[-\frac{1}{M}\nabla_R^2 + E_i(R)\right]\chi(R) = E\chi(R), \tag{12}$$

where M is the proton mass, $E_i(R)$ are the electron energies obtained from Eq. (1), and E is the total (electronic + vibrational) energy of the molecule.

In the electronic continuum, the corresponding nuclear kinetic energy spectra are obtained by projecting onto nuclear Coulomb wave functions, $\chi^c(R)$, as obtained from the solutions of the eigenvalue problem,

$$\left[-\frac{1}{M}\nabla_R^2 + \frac{1}{R}\right]\chi^c(R) = E\chi^c(R), \tag{13}$$

with $1/R$ being the asymptotic potential representing the Coulomb exploding nuclei. The entire source code is available online [18]. The results presented below are also supported by independent calculations made with a fully B-spline based implementation of the problem.

RESULTS

There is a strong coupling between the $1s\sigma_g$ and the $2p\sigma_u$ states in H_2^+. This coupling tends to dominate the one photon dynamics between the ground state and the dissociative p states. In this work we investigate transitions from the electronic ground state to the excited p states, in particular $3p\sigma_u$ and $4p\sigma_u$. The dipole couplings between these states are weak, since the coupling changes sign near $R = 2$ a.u. This is illustrated in Fig. 1, where the relevant dipole couplings are depicted. Figure 2 shows a sketch of the scenario for probing the $1s\sigma_g$-$3p\sigma_u$ coupling. A laser pulse with central frequency $\omega = 0.79$ a.u. pumps population into the $3p\sigma_u$. That photon energy is chosen because it is in resonance at the internuclear distance where the coupling is zero. No transition will occur at that R, but for smaller and larger internuclear distances population will be transferred, and one expects a wave packet containing a minimum to appear on the $3p\sigma_u$. The figure also shows how this wave packet is probed with another laser pulse with $\omega = 0.25$ a.u.

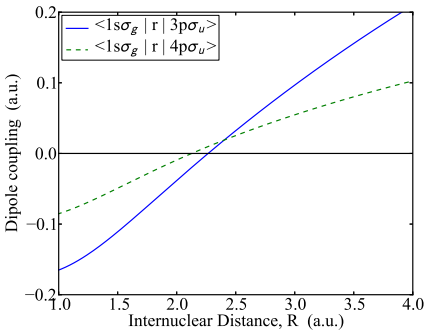

FIG. 1: (color online). The electron dipole coupling between the electronic ground state, $1s\sigma_g$, and the $3p\sigma_u$ (solid line) and $4p\sigma_u$ states (dashed line), respectively, as a function of the internuclear distance.

The upper panel in Fig. 3 depicts the proton energy spectrum on $3p\sigma_u$ that is the result of exposing the vibrational ground state of H_2^+ to a laser pulse of intensity 10^{11} W/cm^2, FWHM duration of ten field cycles, and frequency of $\omega =$ 0.79 a.u. The pulse is not chirped, i.e., $\eta = 0$. The spectrum has a minimum at the proton energy 0.31 a.u., which corresponds to the lack of transition at R = 2.25 a.u. The lower panel in Fig. 3 shows the KER spectrum on $4p\sigma_u$, for a similar laser pulse with frequency $\omega = 0.93$ a.u. This frequency is also chosen because it is in resonance, here between $1s\sigma_g$ and $4p\sigma_u$, at the internuclear distance where the dipole coupling is zero. This occurs at $R = 2.12$ a.u. The probability is an order of magnitude smaller on $4p\sigma_u$, which reflects the size of the coupling shown in Fig. 1. The spectrum on $3p\sigma_u$ has one small peak and one large peak, while the spectrum on $4p\sigma_u$ has two equal-sized peaks. The reason for this is that the laser frequency is resonant at a larger value of R for the transition to $3p\sigma_u$. This is on the tail of the vibrational ground state

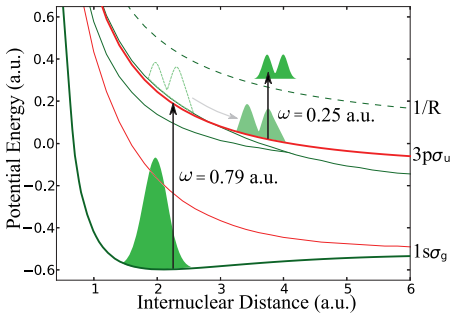

FIG. 2: (color online). Sketch of the pump-probe scenario studied in the present work. A pump pulse ($\omega = 0.79$ a.u.) populates the $3p\sigma_u$ state, and a probe pulse ($\omega = 0.25$ a.u.) ionizes the excited wave packet.

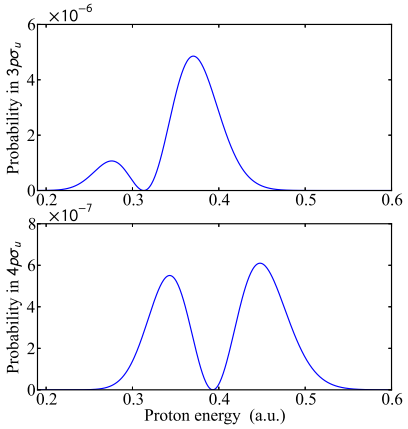

FIG. 3: (color online). Proton energy distribution on $3p\sigma_u$ (upper panel) and $4p\sigma_u$ (lower panel). The H_2^+ molecule started in its vibrational ground state, $1s\sigma_g(v = 0)$, and was exposed to a laser pulse of FWHM duration of ten optical cycles, and an intensity of 10^{11} W/cm^2. The frequency was $\omega = 0.79$ a.u. in the upper panel, and $\omega = 0.93$ a.u. in the lower panel.

wave function, so there is little population at larger internuclear distances, and less population is transferred, resulting in a smaller peak. Since the potential nuclear energy diminishes with larger R, the low peak is for lower energies.

From an experimental point of view, H_2^+ is typically not prepared in the vibrational ground state. It is produced from H_2 that is ionized, and the initial nuclear wave packet is placed at $R = 1.4$ a.u. This Franck-Condon wave packet will oscillate back and forth on the $1s\sigma_g$ potential surface with a characteristic vibrational period. The vanishing coupling to $3p\sigma_u$ can be investigated from the Franck-Condon initial state as well, it may even be beneficial in some respects. Since the wave packet oscillates, it is possible to time the pulse so that the peak will occur when the wave packet is at the internuclear distance of the coupling minimum. This corresponds to letting the laser field peak at $t_i = 133$ a.u. Again, the central laser frequency is $\omega = 0.79$ a.u., the intensity 10^{11} W/cm^2, and the FWHM pulse duration is 10 oscillations. Figure 4 shows the resulting dissociation KER spectrum. The left panels correspond to a $1s\sigma_g(v = 0)$ initial state, while the right panels correspond to a Franck-Condon initial wave packet. The top, middle and lower panels depict the results for chirp parameters η = -1, $\eta = 0$, and $\eta = 1$, respectively. Both the total dissociation energy spectrum (solid line) and the partial contribution from $3p\sigma_u$ (dashed line) are shown. Notice that the $3p\sigma_u$ spectra in the Frack-Condon scenarios have two peaks of equal height, while the peaks in the ground state scenarios are of unequal height. This is because the Franck-Condon wave packet is positioned directly at the R of the coupling node when the field reaches its peak. The minimum in the KER spectra moves from $E = 3.1$ a.u. in the left panels to $E = 3.5$ a.u. in the right panels, presumably because of the inherent kinetic energy in the oscillating wave packet. Three different chirp parameters were applied, and as the figure shows, this does not influence the result on $3p\sigma_u$ much. It does, however, influence the total dissociation spectrum in the Franck-Condon case. When the population is probed by a secondary (probe) pulse, and the energy spectra in the continuum are studied, it makes quite a difference.

It is somewhat challenging to get a clear nuclear signature of the coupling node from the ionized system. Even at the resonance frequency of 0.79 a.u. the populations on $2p\sigma_u$ and $4p\sigma_u$ are of the same order as in $3p\sigma_u$. That means that probing the system with a two-photon transition through $3p\sigma_u$ becomes difficult, since the contribution from $2p\sigma_u$ will drown out the desired signal. Instead, the system is probed with a laser pulse of smaller photon energy, $\omega = 0.25$ a.u., so that the population in $2p\sigma_u$ will not reach the continuum. This resolves most problems when the system is ionized from the ground state. However, when the Franck-Condon initial state is used, another issue appears. Since the initial wave packet is moving, a significant amount of population will reach internuclear distances where the pump pulse may ionize it with one photon. This process will typically overshadow the two-photon ionization signal we are interested in. The problem is solved by chirping the pulse. In a negatively chirped pulse, the high frequency components arrive early in the pulse, before the Franck-Condon wave packet has propagated too far. At the end of the pulse, when much of the wave packet is at

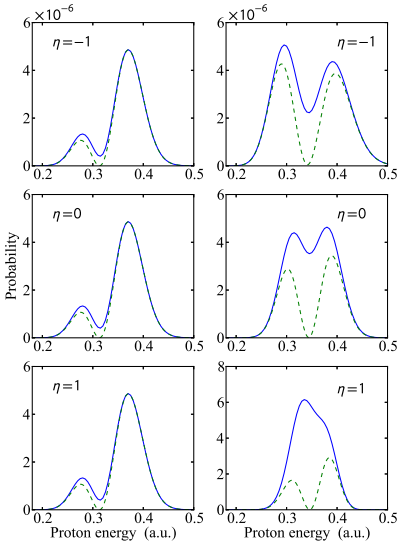

FIG. 4: (color online). Proton energy distribution in the dissociating channels. The H_2^+ molecule started in the vibrational ground state, (left panels), or in a Franck-Condon wave packet on $1s\sigma_g$, (right panels). The laser pulse had a FWHM duration of ten laser oscillations, and an intensity of 10^{11} W/cm^2. The frequency was $\omega = 0.79$ a.u. The chirp parameter of the laser was η = -1 , $\eta = 0$, and $\eta = 1$ in the upper, middle and lower panel, respectively. The dashed line shows the contribution from the $3p\sigma_u$ state.

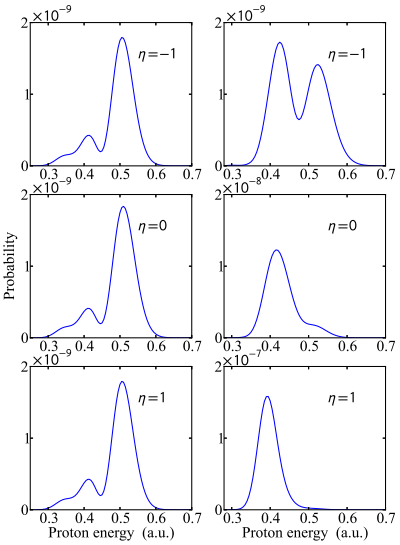

FIG. 5: (color online). Proton energy distribution in the electron continuum. For the panels to the left the H_2^+ molecule was initially prepared in the vibrational ground state, whereas for the right panels it started out in the Franck-Condon state. The chirp parameter of the first laser was $\eta = -1$, $\eta = 0$ and $\eta = 1$ in the upper, middle and lower panel, respectively. The system was exposed to two subsequent laser pulses of intensity 10^{11} W/cm^2. The pump pulse had frequency ω_1 = 0.79 a.u., and FWHM pulse duration, τ_0, corresponding to ten field cycles. The probe pulse had frequency ω_2 = 0.25 a.u., duration six cycles, and no chirp.

large internuclear distances, the photon energy is smaller, and one-photon ionization is still out of reach. This can be observed in Fig. 5.

Figure 5 shows the KER spectra extracted from the electronic continuum after the action of both the pump and probe pulses. The left panels show the results if the $1s\sigma_g(v = 0)$ initial state is used, while the right panels show the results with the Franck-Condon wave packet. The top, middle and bottom panels correspond to the chirp parameters $\eta = -1$, $\eta = 0$ and $\eta = 1$ in the first laser pulse. Both laser pulses had an intensity of 10^{11} W/cm^2. The central frequencies were $\omega_1 = 0.79$ a.u. and $\omega_2 = 0.25$ a.u., and the FWHM durations of the pulses ten and six cycles, respectively. The second pulse was not chirped ($\eta = 0$). Furthermore, the time delay between the pulses was set to 2.8 fs in the calculations. It was found that varying the delay had only little effect on the obtained spectra.

All the energy spectra to the left in Fig. 5, corresponding to ionization from the ground state, show an uneven two-peak shape strikingly similar to the upper panel in Fig. 3, and the left panels in Fig. 4. The shape of the wave function has obviously been well preserved through the probe pulse. The spectra show little dependence on the chirp of the laser. The right panels, on the other hand, show a strong dependence on the chirp. The peak at $E \approx 0.4$ a.u. which becomes dominant in the lower panel, is caused by the one-photon ionization during the first pulse. When the chirp is $\eta = -1$, however, this peak is so small that the two-peak signature from $3p\sigma_u$ dominates.

CONCLUSION

When the H_2^+ system is exposed to chirped pump pulses of frequency ω = 0.79 a.u., double peaked KER spectra appear in the dissociative channels, due to nuclear dynamics on the

$3p\sigma_u$ energy surface. If the system is probed, similarly structured spectra can be extracted from the continuum channels. The energy spectra resemble those reported by Førre *et al.* [9]. The cause of the oscillations in their spectra was an interference between two nuclear wave packets of equal energy, separated by a time delay. The spectra shown here, however, are a result of an electronic two-center interference, that has been carried over to the nuclear wave function. The node on the R-dependent electronic dipole coupling between $1s\sigma_g$ and $3p\sigma_u$ imposes a minimum on the vibrational wave packet that is transferred between the electronic states. The resulting structure in the KER is also found in the continuum channel if the excited system is probed by a second pulse. Both in the dissociation channels, and in the continuum, the simulations with the Franck-Condon initial state result in KER spectra that are strongly dependent on the chirp parameter, while in scenarios with a $1s\sigma_g(v = 0)$ initial state, the spectra are largely unaffected by the chirp. This is a consequence of the unstationary nature of the initial Franck-Condon wave. A chirped pulse has typically the same frequency components as the corresponding unchirped pulse, but their temporal arrangement is different. If the molecular system is evolving, this can strongly influence the result. The KER spectra of the nuclei in the electronic continuum are dominated by a one-photon contribution when the laser chirp is positive. This channel is opened near the end of the pump pulse, because the Franck-Condon wave packet has propagated to large R, and is therefore energetically closer to the electronic continuum. Furthermore, the laser frequency of the positively chirped pulse is then at its highest, making the transition to the continuum possible. A similar effect is responsible for the large $3p\sigma_u$ contribution in the dissociative channel when the chirp is negative. The resonance frequency between $1s\sigma_g$ and $3p\sigma_u$ diminishes with R, and therefore also with time, as the initial wave packet propagates toward larger R. The negatively chirped pulse, where the photon energy abates with time, will be closer to resonance for more of the duration of the pump pulse, resulting in a large population transfer.

* Electronic address: sigurd.askeland@ift.uib.no
† Electronic address: morten.forre@ift.uib.no

[1] A. H. Zewail, Science **242**, 1645 (1988).
[2] A. Staudte, D. Pavičić, S. Chelkowski, D. Zeidler, M. Meckel, H. Niikura, M. Schöffler, S. Schössler, B. Ulrich, P. P. Rajeev, T. Weber, T. Jahnke, D. M. Villeneuve, A. D. Bandrauk, C. L. Cocke, P. B. Corkum, and R. Dörner, Phys. Rev. Lett. **98**, 073003 (2007).
[3] S. Chelkowski, A. D. Bandrauk, A. Staudte, and P. B. Corkum, Phys. Rev. A **76**, 013405 (2007).
[4] M. Vafaee, Phys. Rev. A **78**, 023410 (2008).
[5] H. A. Leth, L. B. Madsen, and K. Mølmer, Phys. Rev. Lett. **103**, 183601 (2009).
[6] B. Fischer, M. Kremer, T. Pfeifer, B. Feuerstein, V. Sharma, U. Thumm, C. D. Schröter, R. Moshammer, and J. Ullrich, Phys. Rev. Lett. **105**, 223001 (2010).
[7] D. Pavičić, A. Kiess, T. W. Hänsch, and H. Figger, Phys. Rev. Lett. **94**, 163002 (2005).
[8] B. D. Esry, A. M. Sayler, P. Q. Wang, K. D. Carnes, and I. Ben-Itzhak, Phys. Rev. Lett. **97**, 013003 (2006).
[9] M. Førre, S. Barmaki, and H. Bachau, Phys. Rev. Lett. **102**, 123001 (2009).
[10] V. Mezoui Ndo, L. O. Owono, B. Piraux, S. Barmaki, M. Førre, and H. Bachau, Phys. Rev. A **86**, 013416 (2012).
[11] S. Selstø, M. Førre, J. P. Hansen, and L. B. Madsen, Phys. Rev. Lett. **95**, 093002 (2005).
[12] S. Barmaki and H. Bachau, J. Phys. B **40**, 463 (2007).
[13] M. Born and R. Oppenheimer, Annalen der Physik **84**, 457 (1927).
[14] G. L. Kamta and A. D. Bandrauk, Phys. Rev. A **71**, 053407 (2005).
[15] C. de Boor, *A practical Guide to Splines*, revised ed. (Springer-Verlag, New York, 2001).
[16] H. Bachau, E. Cormier, P. Decleva, J. E. Hansen, and F. Martín, Rep. Prog. Phys. **64**, 1815 (2001).
[17] L. F. Shapine and M. K. Gordon, *Computer Solution of Ordinary Differential Equations* (W.H. Freeman, San Francisco, 1975).
[18] S. Askeland, https://github.com/sas044/H2plus_Born_Oppenheimer (2013), project source code.